Title

Uncorrelated Bi off-centering and the insulator-to-metal transition in ruthenium A2Ru2O7
pyrochlores

Journal

Physical Review Materials, 3(9)

ISSN

2475-9953

Authors

Laurita, Geneva
Puggioni, Danilo
Hickox-Young, Daniel
et al.

Publication Date

2019-09-17

DOI

10.1103/PhysRevMaterials.3.095003

Peer reviewed

Uncorrelated Bi off-centering and the insulator-to-metal transition in ruthenium $A_2Ru_2O_7$ pyrochlores

Geneva Laurita*
Department of Chemistry and Biochemistry, Bates College, Lewiston, Maine 04240, United States

Danilo Puggioni, Daniel Hickox-Young, and James M. Rondinelli
Department of Materials Science and Engineering, Northwestern University, Evanston IL, 60208, USA

Michael W. Gaultois
Leverhulme Research Centre for Functional Materials Design, The Materials Innovation Factory
Department of Chemistry, University of Liverpool, 51 Oxford Street, Liverpool, L7 3NY, United Kingdom

Katharine Page
Chemical and Engineering Materials Division, Oak Ridge National Laboratory, Oak Ridge, TN 37831

Leo K. Lamontagne and Ram Seshadri
Materials Department and Materials Research Laboratory, University of California, Santa Barbara, CA 93106
(Dated: September 17, 2019)

The study of insulator-to-metal transitions is of interest from the viewpoint of fundamental understanding of the underlying physics, and materials at the brink of such transitions possess useful functionality. Driving this transition through compositional tuning can help engineer useful material properties. Here we study the role of disorder in the form of cation off-centering on the compositionally-controlled insulator-to-metal transition in the solid solution oxide pyrochlore $(Pr_{1-x}Bi_x)_2Ru_2O_7$. Prior work has established site disorder by the Bi^{3+} cations shifting incoherently away from their ideal crystallographic site in the Bi end-member pyrochlore as a consequence of stereochemical activity of the lone pair of electrons. However, less is known about the consequences of such off-centering in solid solutions and its role in determining the electronic ground state. Here we demonstrate through total scattering studies that even a small substitution of Bi on the pyrochlore *A* site leads to site disorder that enhances the average effective size of the *A*-site cation. This indirectly increases Ru–O–Ru covalency, which appears to play a crucial role in the cross-over from insulating to metallic behavior in the solid solution. Further, density functional electronic structure calculations suggest the combination of primary and secondary (due to size) electronic effects of the lone pair-driven incoherent cation displacements drive the solid solution into a metallic state.

I. INTRODUCTION

Complex oxides of the 4*d* transition metals — exemplified by oxides of Ru — are of interest because of the diminished extent of electron correlation compared to the more widely studied 3*d* metal oxides, the enhanced role of spin-orbit coupling, and the greater prevalence of orbital degeneracy. Among the novel electronic and magnetic properties arising from the nature of the 4*d* electrons are "clean" electrical conductivity in KRu_4O_8,[1–4] spin-glass behavior in $Ca_2Ru_2O_7$,[5] superconductivity in Sr_2RuO_4,[6] and simultaneous metallic conductivity and ferromagnetism in $SrRuO_3$.[7–10] In particular, ruthenium pyrochlores have been studied for applications as electrode materials,[11] catalysts for oxygen evolution and oxygen reduction reactions,[12,13] materials in high-capacity Li batteries,[14] and components of thick-film resistors.[15] In these applications, electrical transport plays an important role in determining the viability of the material towards device application. However, there are still open questions with regard to electrical transport and magnetic ground states in $A_2Ru_2O_7$ (*A* = Pr, ... , Lu, Y, Bi, Pb, Tl *etc.*) pyrochlores.

The pyrochlore structure type, illustrated in Fig. 1, can be represented by the formula $A_2B_2O_6O'$ with two crystallographically distinct oxygen positions: O in the 48*f* Wyckoff position at $(x, \frac{1}{8}, \frac{1}{8})$ and O′ in the 8*b* site at $(\frac{3}{8}, \frac{3}{8}, \frac{3}{8})$.[16] The structure is commonly described as two interpenetrating networks of (i) a diamond sublattice A_2O' and (ii) a corner-connected network of BO_6 octahedra.[16,17] The BO_6 network forms a fairly rigid channel in which the A_2O' chains are interspersed, and the channel allows for several modifications of the pyrochlore structure type in the form of nonstoichiometry on the *A* and O′ sites.

The pyrochlore structure type is additionally tolerant to positional and site disorder of both *A* and O′ sites, which may be difficult to determine through traditional crystallographic techniques such as neutron or X-ray diffraction. For example, both metallic $Bi_2Ru_2O_7$[18] and insulating $Bi_2Ti_2O_7$[18,19] exhibit apparent crystallographic disorder of the Bi cations observed as enlarged anisotropic atomic displacement parameters from Rietveld refinement of diffraction data. However, through the application of the neutron pair distribution function (PDF), which provides a real-space atom-atom correla-

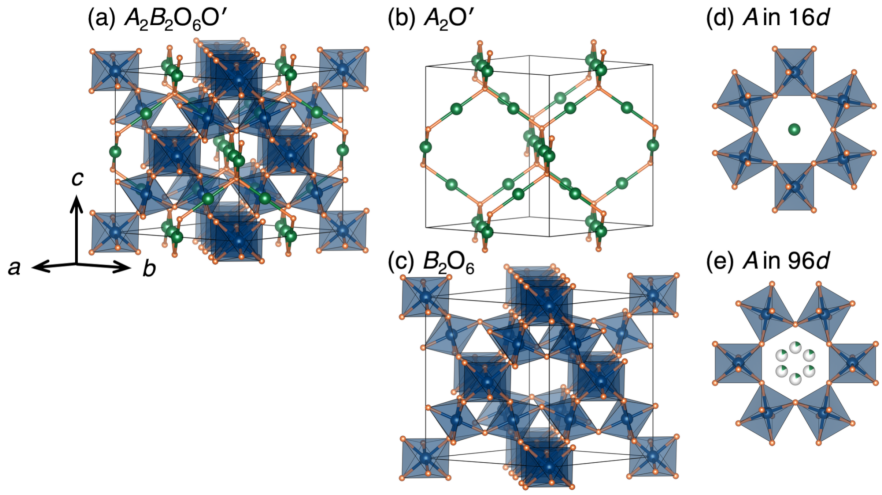

FIG. 1. (a) The $A_2B_2O_6O'$ pyrochlore structure comprising interpenetrating networks of (b) a diamond A_2O' sublattice and (c) a sublattice of corner-connected BO_6 octahedra. (d) The ideal A-site 16d position in the center of the BO_6 channel compatred with (e) the off-centered (disordered) 96g position.

tions and therefore a view of the *local* structure, it was determined that in both materials this apparent disorder arises from incoherent, local off-centering of the Bi^{3+} cations due to stereochemical activity of the associated lone pair of $6s^2$ electrons.[18] The application of local techniques such as PDF and X-ray absorption spectroscopy (XAS) provides crucial insight on the nature of the disorder in a material, which can influence the observed properties, as demonstrated in various ruthenium oxide materials.[20,21] The incoherent off-centering of the A-site, and the frequent absence of ordered distorted structural ground states in this structure type could potentially be linked to frustration arising from the topology,[22] in analogy with the difficulty of obtaining long-range spin-ordered ground states.[23,24]

The electronic properties of $A_2Ru_2O_7$ pyrochlores arise from the corner-sharing RuO_6 sublattice.[25–27] Metallic character originates from π-type orbital interactions of Ru 4d and O 2p orbitals across the Ru–O–Ru bridges of the corner-shared octahedra. A combination of an increase in the size of the A-site cation and shorter Ru–O bonds results in an increase in the Ru–O–Ru orbital overlap, facilitating greater interaction and promoting metallic transport behavior.[25] Insulating ruthenium pyrochlores such as $Yb_2Ru_2O_7$ and $Lu_2Ru_2O_7$ exhibit Ru–O–Ru bond angles of 127 ° and 132 °, respectively, whereas metallic $Bi_2Ru_2O_7$ has an increased bond angle of 133 °.[28]

In the lanthanide ruthenium pyrochlores, the room temperature electrical resistivity decreases uniformly with increasing ionic radius of the lanthanide cation.[29] However, the introduction of any Bi^{3+} leads to substantial deviation from the trend created simply by size of the A-site as seen from tuning rare-earth radii, suggesting there are contributions other than size effects. The $6s^2$ lone pair distinguishes Bi^{3+} from the Ln^{3+} lanthanide ions that lead to insulating behavior. Previous Reverse Monte Carlo (RMC) analysis of neutron total scattering data collected from $Bi_2Ti_2O_7$ and $Bi_2Ru_2O_7$ revealed Bi nuclei are locally displaced from the average position described by the cubic pyrochlore crystal structure,[18,19] driven by stereochemical activity of the Bi lone pair.

Here we examine how the increase in the A-site cation radius results in a corresponding increase in the Ru–O–Ru bond angle, driving the system towards metallic behavior. We hypothesize that the local distortion caused by Bi cations is responsible for the observed metallic behavior and the distinct behavior of the Bi-containing pyrochlores when contrasted with the lanthanide end members. We employ neutron total scattering techniques and least-squares modeling to determine the influence of Bi^{3+} on the local structure in the series $(Pr_{1-x}Bi_x)_2Ru_2O_7$ ($x = 0.0$, 0.1, 0.5, and 1.0). We find the Bi^{3+} are displaced from their ideal sites in all Bi-containing samples, influencing the effective size of the A-site cation and the resulting structural and physical properties throughout the series. The study is complemented with density functional theory (DFT)-based electronic structure calculations carried out on the ideal structure as well as structural models that represent the local off-centering disorder seen in experiment. The trends in the densities of states provide insights into the observed transport behavior.

II. METHODS

Polycrystalline samples were prepared by direct reaction of constituent oxide powders (RuO_2, 99.99%, Sigma-Aldrich; Pr_6O_{11}, 99.99%, Alfa Aesar; Bi_2O_3, 99.99%, Alfa Aesar) with multiple firings. Powders were ground using an agate mortar and pestle, pressed into

13 mm diameter pellets using a uniaxial pellet press, and placed in a dense alumina crucible on a sacrificial bed of powder of the same composition. Samples were reground and pelleted between all firings.

$Bi_2Ru_2O_7$ was prepared by heating in air from room temperature to 1003 K over 3 h, annealing for 24 h and cooling to room temperature in the furnace. This was repeated once, followed by a 24 h firing 1073 K. $Pr_2Ru_2O_7$ was prepared by heating in a box furnace in air from room temperature to 1173 K over 3 h, annealing for 24 h, and cooling to room temperature in the furnace. This process was repeated 4 times. Owing to the low melting point of Bi_2O_3, Bi-containing samples were prepared by heating in air from room temperature to 1003 K over 3 h, annealing for 24 h and cooling to room temperature in the furnace. This was repeated 2 times, followed by 2 additional 24 h firings at 1073 K, and 3 additional 24 h firings at 1173 K.

All samples were then annealed in a tube furnace at 1373 K (1173 K for $Bi_2Ru_2O_7$) for 12 h under flowing ultra-high-purity Ar further purified using a Ti gettering furnace, and cooled to room temperature under Ar at 2 K min^{-1}. Owing to the volatility of Ru oxides in air at high temperatures ($T \sim 1313$ K)[29], these high(er) temperature annealing steps were performed under Ar.

Time-of-flight (TOF) neutron total scattering data were collected on powdered samples at the NPDF instrument at Los Alamos National Laboratory.[30] 3 g to 4 g of sample was placed into a vanadium can, and measurements were performed at 298 K for approximately 4 h. Rietveld refinements of the neutron diffraction data were conducted using the GSAS software with the interface EXPGUI.[31,32] Data reduction to obtain the PDF $G(r)$ function was performed using the PDFgetN program[33] with $Q_{\max} = 35$ Å^{-1}, which was selected to balance between resolution and termination ripples in the reduced data. Least-squares refinement of the PDF data were performed with PDFGUI[34] over a range of 1.7 Å to 5 Å. Crystal structures were visualized using the VESTA software suite.[35]

First-principles DFT calculations employed the Perdew-Burke-Ernzerhof exchange-correlation functional revised for solids (PBEsol)[36] as implemented in the Vienna *Ab initio* Simulation Package (VASP)[37] with the projector augmented wave (PAW) approach[38] to treat the core and valence electrons using the following electronic configurations: $2s^2 2p^4$ (O), $4p^6 4d^7 5s^1$ (Ru), $5s^2 5p^6 6s^2 5d^1$ (La), $5s^2 6s^2 5p^6 5d^1$ (Pr, Nd, and Sm), $6s^2 5p^6 5d^1$ (Lu) and $6s^2 5d^{10} 6p^3$ (Bi). A $6 \times 6 \times 6$ Γ-centered k-point mesh was generated and a 650 eV energy cutoff was used for the planewaves. For all calculations, the atomic positions were relaxed (forces <0.1 meV Å^{-1}) using Gaussian smearing (20 meV width) and the experimental lattice constants reported herein.

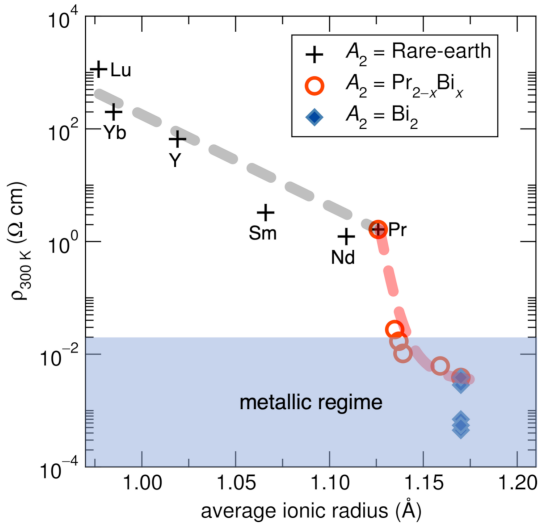

FIG. 2. Room temperature resistivity ($\rho_{300\,K}$) as a function of the average A-site ionic radii for the series $(Pr_{1-x}Bi_x)_2Ru_2O_7$ (x=0.0, 0.1, 0.5, and 1.0), shown in filled squares, illustrates a cross-over from insulating to metallic conductivity between x=0.1 and x=1.0. The data is compared to literature on other $A_2Ru_2O_7$ pyrochlores,[29,39–43] and follows expected trends.

III. RESULTS AND DISCUSSION

A recent compilation was created of the trends in room-temperature electrical resistivity[29] ($\rho_{300\,K}$) as a function of A-site ionic radii (for 3+ cations in 8–coordination[44]) from the extensive pyrochlore literature.[16,26,39,40,42,45–47] When A = rare earth, there is a simple trend of a logarithmic decrease in the room temperature resistivity taking the materials closer to metallicity, as the rare-earth radius increases. Data on the series $(Pr_{1-x}Bi_x)_2Ru_2O_7$ ($x = 0.0, 0.1, 0.5, 1.0$) with Bi^{3+} substitution behaves anomalously. Samples with $x = 0.0$ and $x = 0.1$ exhibit electrical resistivity above the metallic threshold, while a rapid crossover into the metallic regime is observed at room temperature for the $x = 0.5$ and $x = 1.0$ samples, at a rate not explained simply by an averaging of the size of A-site ions.

To investigate the transition to metallic behavior with increasing Bi content from both an average, crystallographic and local perspective, neutron total scattering data was collected at 300 K. Rietveld refinements of the data indicate all samples can be indexed to the $Fd\bar{3}m$ space group, and the data is well described by the cubic pyrochlore structure. Refined occupancies are close to the nominal values within error, with the exception of Bi and O′ vacancies in the nominal $Bi_2Ru_2O_7$ compound. Vacancies in both the Bi and 8b oxygen sites appear to be intrinsic for the Bi end member, and has been reported in the literature.[18,48–50] These vacancies decrease as the solid solution progresses towards the Pr-rich end. A summary of the refined crystallographic data is presented in Table I, and a summary of the refined atomic data is pre-

TABLE I. Crystallographic information from the Rietveld refinements of neutron diffraction data of $(Pr_{1-x}Bi_x)_2Ru_2O_7$ at 300 K.

Source	neutron TOF	neutron TOF	neutron TOF	neutron TOF
Chemical formula	$Pr_2Ru_2O_7$	$Pr_{1.83(2)}Bi_{0.17(2)}Ru_2O_7$	$Pr_{1.12(2)}Bi_{0.88(2)}Ru_2O_{6.94}$	$Bi_{1.92(1)}Ru_2O_{6.88(1)}$
Formula weight	595.95	607.67	578.24	712.02
Temperature (K)	300	300	300	300
Crystal system	cubic	cubic	cubic	cubic
Space Group	$Fd\bar{3}m$	$Fd\bar{3}m$	$Fd\bar{3}m$	$Fd\bar{3}m$
a (Å)	10.3689(5)	10.3607(3)	10.3299(5)	10.2969(5)
Volume (Å^3)	1114.8(5)	1112.17(9)	1102.28(5)	1091.76(3)
Z	8	8	8	8
d-space range (Å^{-1})	0.491 to 7.095	0.491 to 7.097	0.491 to 7.097	0.492 to 7.097
χ^2	15.64	18.63	12.22	17.43
R_p (%)	3.11	3.09	2.52	2.76
R_{wp} (%)	4.77	4.65	3.95	4.28

TABLE II. Select refined atomic parameters from the Rietveld refinements of neutron diffraction data of $(Pr_{1-x}Bi_x)_2Ru_2O_7$ at 300 K.

Chemical formula	$Pr_2Ru_2O_7$	$Pr_{1.83(2)}Bi_{0.17(2)}Ru_2O_7$	$Pr_{1.12(2)}Bi_{0.88(2)}Ru_2O_{6.94}$	$Bi_{1.92(1)}Ru_2O_{6.88(1)}$
O x	0.3292(2)	0.3286(5)	0.3277(5)	0.3271(5)
Ru–O–Ru (°)	131.69(5)	132.01(5)	132.54(5)	132.83(5)
A U_{xx} (Å^2)	0.0038(5)	0.0053(7)	0.0114(7)	0.0160(7)
A U_{xy} (Å^2)	−0.0011(7)	−0.0014(6)	−0.0042(6)	−0.0055(5)
Ru U_{iso} (Å^2)	0.0009(3)	0.0016(3)	0.0015(3)	0.0029(3)
O1 U_{iso} (Å^2)	0.0032(2)	0.0044(2)	0.0053(2)	0.0067(2)
O2 U_{iso} (Å^2)	0.0026(6)	0.0039(6)	0.010(8)	0.017(5)
Bi occupancy	0	0.08(2)	0.44(2)	0.97(5)
O2 occupancy	1.0	1.0	0.93(2)	0.88(3)

sented in Table II.

The trends in refined parameters upon Bi-substitution is illustrated in Fig. 4, presented as a function of increasing Bi content. Lattice parameters decrease with increasing Bi content (Fig. 4a), which counters the trend expected when replacing smaller Pr^{3+} (ionic radii of 1.13 Å in an 8 coordinate site) with Bi^{3+} (ionic radii of 1.17 Å in an 8 coordinate site).[44] This is a direct result of the chemical properties of Bi, and directly influences the observed metallic behavior in the Bi-rich samples.[28] The presence of the softer Bi cation leads to a shift in the 48f O atomic position (Fig. 4b), which leads to a larger Ru–O–Ru bond angle (Fig. 4c). This enhances the Ru 4d and O 2p orbital overlap, thus shortening the Ru–O bond length and the unit cell dimensions.

The atomic displacement parameters (ADPs) of the *A*-site cations were modeled anisotropically (U_{ani}) to determine if any directionality was present in the atomic displacements. Upon Bi substitution, displacement towards the edge of the surrounding RuO_6 octahedra is observed, perpendicular to the channel formed by the octahedral network (Fig. 5). The magnitude of this perpendicular displacement, described by the $U_{11,22,33}$ components of the U_{ani}, increases with Bi content (Fig. 4d), indicating that more disorder on the *A*-site is observed when Bi is present. Both the directionality and magnitude of the anisotropic displacements upon increasing Bi content point towards the stereochemical activity of the $6s^2$ lone pair of electrons associated with Bi^{3+} and subsequent off-centering of the *A*-site cation.

To better understand the nature of the observed disorder on the *A* site, analysis of the neutron PDF was performed against two crystallographic models: the 16d model where the *A*-site cations are placed in the center of the channel in the 16d Wyckoff position at ($\frac{1}{2}$, $\frac{1}{2}$, $\frac{1}{2}$) and the 96*g* model where the *A*-site cations are allowed to off-center in the channel in the 96*g* Wyckoff position at (x, x, z). These are respectively displayed in panels (d) and (e) of Fig. 1. The neutron PDF data for all samples were fit over a range of 1.5 Å to 5.0 Å against both the 16d and 96*g* models, shown in Fig. 6 for the $x = 0.5$ and 1.0 samples. All samples are well described by the

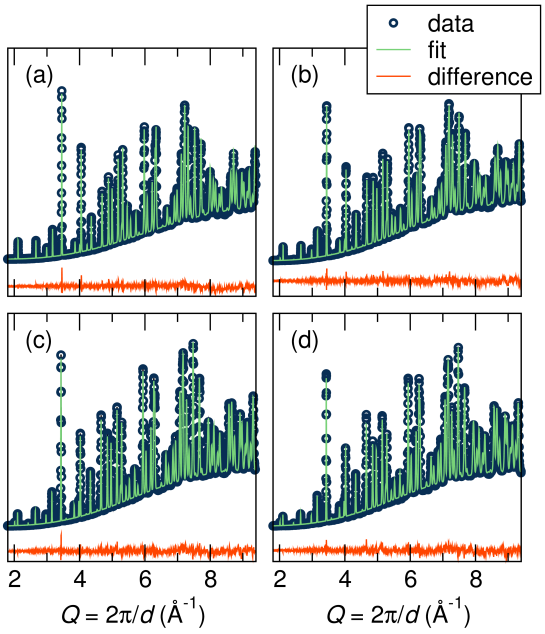

FIG. 3. Rietveld refinements of the neutron diffraction data (NPDF, Los Alamos National Laboratory) for the series $(Pr_{1-x}Bi_x)_2Ru_2O_7$ [(a) $x = 0.0$, (b) $x = 0.1$, (c) $x = 0.5$, and (d) $x = 1.0$] indicates all samples can be crystallographically described by the cubic pyrochlore structure with space group $Fd\bar{3}m$ (no. 227).

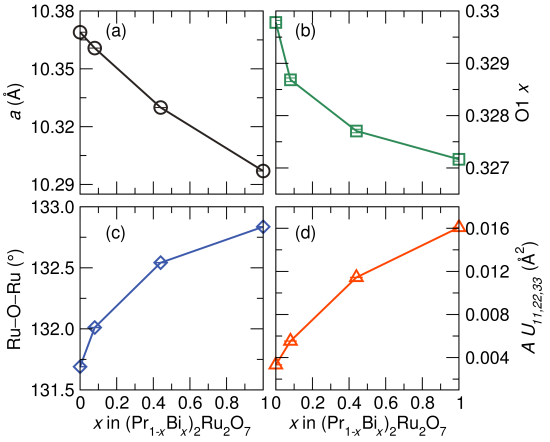

FIG. 4. Refined parameters from Rietveld refinement of neutron diffraction data. (a) Cell parameter a, (b) O1 variable x position, (c) Ru–O–Ru bond angle, and (d) anisotropic atomic displacement parameters (ADPs) of the *A*-site cation as a function of Bi content. A contraction of the lattice parameter, shift in the O1 position, and increase in the Ru–O–Ru bond angle are observed with increasing Bi content due to an increase in the covalency of the Ru–O bonds. An increase in the anisotropic ADPs indicates increased disorder on the *A*-site with increasing Bi content.

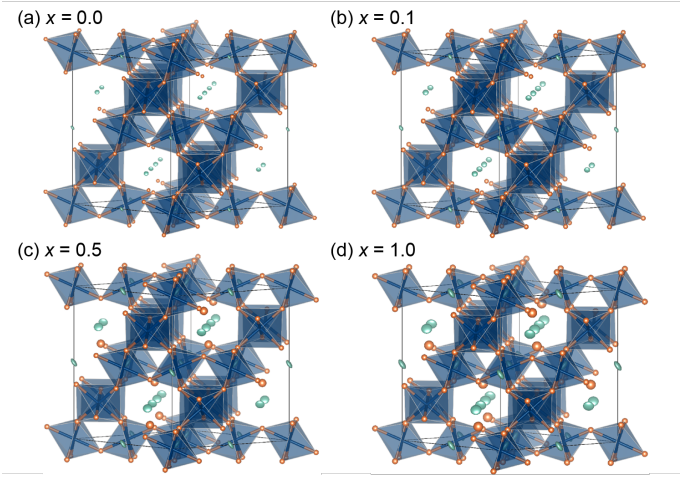

FIG. 5. Crystallographic structures for the series $(Pr_{1-x}Bi_x)_2Ru_2O_7$ [(a) $x = 0.0$, (b) $x = 0.1$, (c) $x = 0.5$, and (d) $x = 1.0$] indicates anisotropic ADPs of the *A*-site cation (shown at 90 % probability) increase with Bi concentration.

16d model, but fits of the $x = 0.5$ and 1.0 data are visibly improved below 3 Å with the 96g model. The refined parameters from the two models are plotted in Fig. 7 as a function of Bi content. Both the 48f O positional parameter and Ru–O–Ru bond angle are similar for both models, and in agreement with the trends observed through analysis of the diffraction data. However, a clear difference in the success of the two models is seen in comparing the goodness-of-fit parameter R_w and Bi U_{iso} in the Bi-rich samples, both of which are lowered with the 96g model. Combined, these parameters suggest the 96g model is a better description of the behavior of the *A*-site cations when Bi is present. For the Bi end member, a maximum displacement of 0.16 Å from the center of the channel is observed, in agreement with values obtained in the literature.[48] This off-centering indicates the $6s^2$ lone pair is stereochemically active, resulting in a larger effective radius of the *A* site, and subsequent widening of the Ru–O-Ru bond angle, which in turn, gives rise to an enhanced bandwidth for the conduction band created from Ru and O states.

Analysis of both the average and local structure by means of neutron total scattering suggests with increasing Bi content the system progressively deviates from a simple model where the *A*-site atom occupies the ideal position; *A*-site off-centering and local disorder increases continuously. However, these models are based on the assumption that all *A*-site ions behave identically, and it is not clear whether Bi is strongly locally displaced at all levels of substitution, or whether the displacement gradually increases with substitution. Particularly at low levels of Bi substitution, the total scattering is not sensitive to the small amount of Bi on the *A*-site, as the contribution is a weighted average of Pr/Bi. Regardless, it is apparent that even with small amounts of bismuth substitution, disorder is induced on the *A*-site despite Pr^{3+} and Bi^{3+} having fairly similar ionic radii, and the disorder plays a role in the effective size of the site in the structure. However, the local Ru–O–Ru bond angle evolution

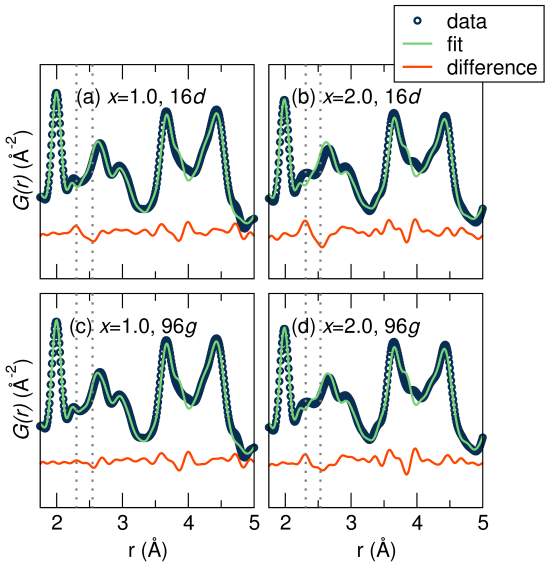

FIG. 6. Fits of the neutron PDF (NPDF, Los Alamos National Laboratory) against (a,b) the crystallographic structure with the *A*-site cation in the ideal 16*d* Wyckoff site at (0.5,0.5,0.5) and (c,d) with the *A*-site cation displaced into the 96*g* Wyckoff site at (x, x, z). For both the $x = 0.5$ (a,c) and $x = 1.0$ (b,d) samples the data is better described by the 96*g* model, suggesting the *A*-site cations are displaced from the ideal crystallographic site, a result of stereochemical activity of the $6s^2$ lone pairs associated with Bi^{3+}. Dashed lines indicate *A*–O bond lengths when the *A*-site cation is placed in the ideal 16*d* position.

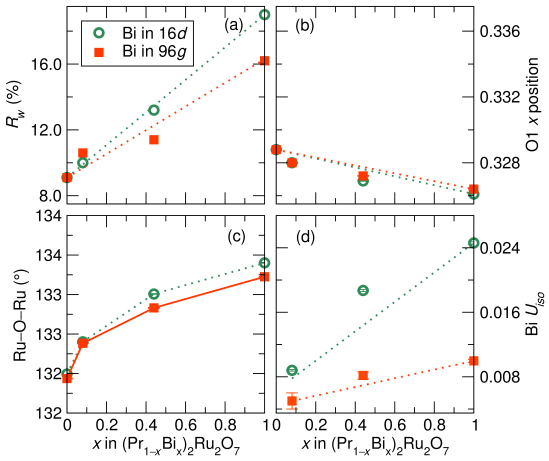

FIG. 7. Comparison of the refined data from fits of the NPDF data against the 16*d* and 96*g* models as a function of increasing Bi content. (a) For all Bi-containing samples, a lower goodness-of-fit parameter, R_w, is obtained with the 96*g* model, suggesting the local structure is best described by the displaced model. (b) O1 x position is relatively unaffected by the two models, supporting that the models are solely a modification of the *A*-site cation. (c) Ru–O–Ru bond angles are additionally similar for both models, whereas (d) isotropic ADPs of the *A*-site cation are significantly lowered in the 96*g* displaced model, indicating this model approximates a better description of the local structure.

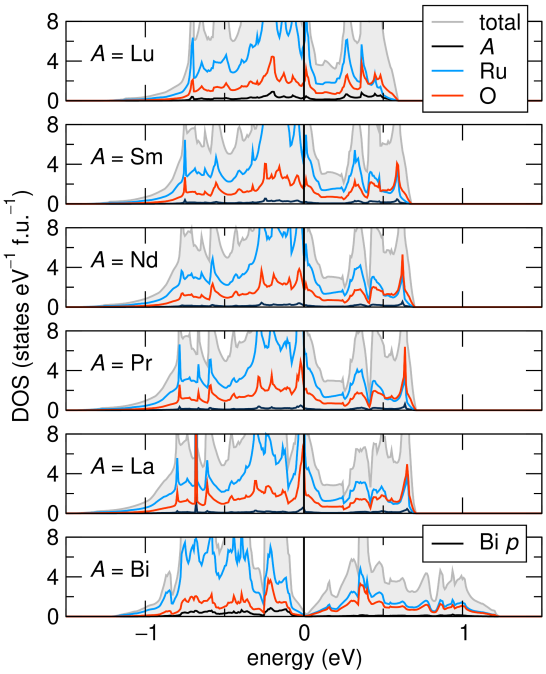

FIG. 8. (a) Total and projected density of states (DOS) for $Ln_2Ru_2O_7$ (Ln = Lu, Sm, Nd, Pr, and La) and $Bi_2Ru_2O_7$. The energies are referenced to the Fermi at 0 eV (vertical line).

follows a similar trend of a relatively small increase with Bi substitution, suggesting that more than sterics are at play for the observed electrical properties.

In order to relate the structural evolution to electronic properties, we performed DFT calculations of the electronic structure to examine the role of local structure on the low-energy electronic densities of states (DOS), which in turn, impacts electrical transport. The total and projected densities-of-states (DOS) for $Ln_2Ru_2O_7$ and $Bi_2Ru_2O_7$ with the cubic $Fd\bar{3}m$ space group are presented in Fig. 8. For all the compounds, consistent with low-spin Ru^{4+}, the valence band is composed largely of Ru t_{2g}^4 states hybridized with O 2*p* states. The $Ln_2Ru_2O_7$ (Ln = Lu, Sm, Nd, Pr, and La) compositions exhibit relatively narrow and populous states at the Fermi level (E_F) at the DFT-PBEsol level, consistent with the potential for electron correlation driving insulating and magnetic behavior. In contrast, $Bi_2Ru_2O_7$ exhibits fewer and less peaked DOS — almost pseudogapped[48] — with a redistribution of states above and below E_F that acts to renormalize the orbital bandwidth. The pseudogap opening near E_F originates from a localized feature in the energy range of -25 meV with respect to E_F, wherein the strong hybridization between Ru 4*d* and O 2*p* states is modulated by the Bi 6*p* states through the additional hybridization of Bi 6*p* and Ru t_{2g}^4 states.

Figure 9 presents the Ru t_{2g} bandwidth evolution as a function of DFT calculated Ru–O–Ru bond angles in $Ln_2Ru_2O_7$ and $Bi_2Ru_2O_7$. For all of these calculations, the ideal crystallographic structures were employed, with no displaced atoms. In $Ln_2Ru_2O_7$, the band-

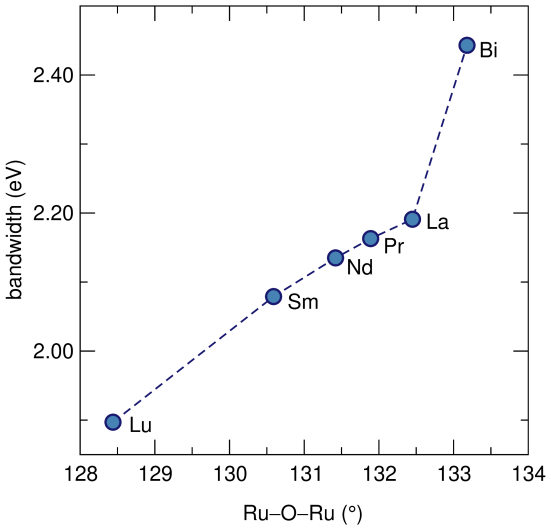

FIG. 9. Bandwidth values of the Ru t_{2g} bands as a function of the Ru–O–Ru bond angles in $Ln_2Ru_2O_7$ (Ln = Lu, Sm, Nd, Pr, and La) and $Bi_2Ru_2O_7$ extracted from DFT electronic structures.

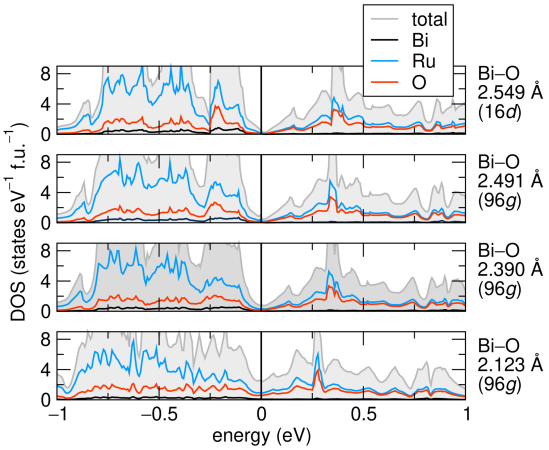

FIG. 10. (a) Total and projected density of states (DOS) for stoichiometric $Bi_2Ru_2O_7$ as a function of the Bi^{3+} displacements from the $16d$ to $96g$ Wyckoff site. The energies are referenced to the Fermi at 0 eV (vertical line).

widths increase linearly as a function of the Ln^{3+} ionic radii and Ru–O–Ru bond angles. Although the difference in the Ru–O–Ru bond angles for $Bi_2Ru_2O_7$ and $La_2Ru_2O_7$ is less than 1°, the bandwidth of $Bi_2Ru_2O_7$ is significantly larger, and markedly deviates from the trend followed by the other compounds in accordance with the reported room temperature electrical resistivities of $Ln_2Ru_2O_7$ and $Bi_2Ru_2O_7$ (see Fig. 2). Going from $Ln_2Ru_2O_7$ to $Bi_2Ru_2O_7$ it would appear that two things happen: The density of states is no longer peaked at E_F and the width of the band contributing charge carriers is enlarged. Both of these effects would suggest that while $Ln_2Ru_2O_7$ are susceptible to electronic instabilities leading to magnetic and insulating ground states, $Bi_2Ru_2O_7$ is a candidate for metallic behavior.

We anticipate the conductivity to be robust to small amounts of oxygen vacancies as observed in our samples. Previous work on stoichiometric samples of $Bi_2Ru_2O_7$ (determined through compositional analysis[51] and neutron scattering[18]) report the same metallic conductivity as samples with vacancies, suggesting the enhanced metallicity is not an effect of the observed vacancies.

To examine how the $Bi_2Ru_2O_7$ electronic structure is impacted by local off-centering of Bi^{3+} cations, we have computed the electronic properties while constraining the Ru–O–Ru bond angles to 133.18°, simulating the experimental displacements of the Bi^{3+} cations in the "$96g$" model (Fig. 10). When the Bi^{3+} cations occupy the $16d$ Wyckoff site at $(1/2, 1/2, 1/2)$, the Bi–O bond length is ~ 2.6 Å and $Bi_2Ru_2O_7$ appears to be semimetallic with a pseudogap opening at E_F (Fig. 10, top panel). A more careful analysis of the DOS reveals strongly localized states at the top of the valence band, in the energy range of -25 meV of E_F, wherein the hybridization between Ru $4d$ and O $2p$ states is mediated by partially filled Bi $6p$ states, which should nominally be empty. This results in strong covalent Ru–O bonds, as also suggested by the calculated electron localization function (ELF) shown in Fig. 11(a), and is robust to the effects of spin-orbit interactions.

The displacement of the Bi^{3+} cations into the $96g$ Wyckoff site to (x, x, z) shortens the Bi–O bond length, increasing the number of states at E_F (Fig. 10 three lower panels). In particular, when the Bi–O bond length is ≈2.1 Å, the number of states at the Fermi level increases to $N(E_F) \approx 2.5$ states eV^{-1} f.u.$^{-1}$. Note that in the neutron PDF data (Fig. 6) the lowest boundary of the Bi–O peak sets the minimum Bi–O bond distance to 2.1 Å. The local off-centering of the Bi^{3+} cations reduces the weight of the Bi $6p$ states in the valence band, decreasing the localization of the Ru $4d$ and O $2p$ states at the top of the valence band. The Bi off-centering and weak $6p$ hybridization results in a lower degree of covalency of the Ru–O bonds [Fig. 11(b)] with consequent enhanced metallic behavior. The pseudo-gap that occurs when Bi is centered in the $16d$ position arises from strong Bi $6p$ and Ru t_{2g}^4 hybridization, which strengthens the covalency of the Ru–O bond. Consequently, the nominally empty Bi $6p$ states are then partially occupied in the sense that they form part of the bonding state involved in the covalent bond. When the Bi atom displaces away from the $16d$ position, the Ru–O bonding interaction is weakened and the gap closes, enhancing the metallicity. This behavior points to the dual role of Bi^{3+} cations in the electronic properties of $Bi_2Ru_2O_7$: cation off-centering favors enhanced metallicity *via* decreased orbital occupation in addition to the off-centering effectively enlarging the Ru–O–Ru bond distances resulting in more delocalized charge carriers. Together, these effects account for the dramatic changes in the electrical behavior upon Bi substitution.

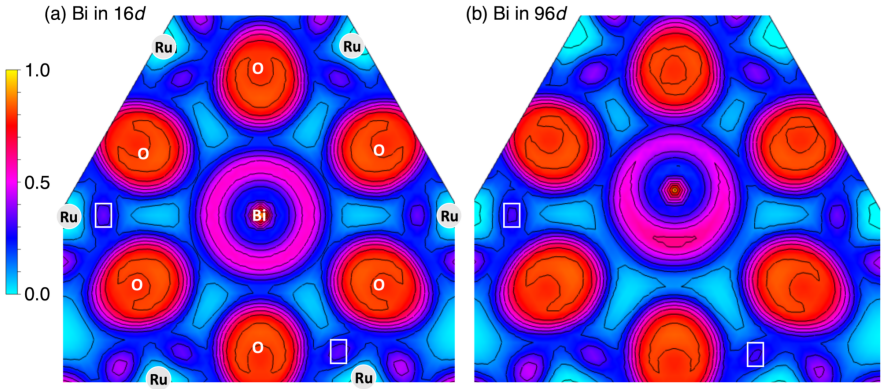

FIG. 11. (a) Electron localization function (ELF) of $Bi_2Ru_2O_7$ with Bi^{3+} cations in the 16d and (b) mimicked 96g position. The white boxes highlight the difference in covalency of the Ru–O bonds.

We would imagine that since this role of Bi^{3+} is local, it would persist in any solid solution of Ln^{3+} and Bi^{3+} which could help explain why Bi^{3+} is a "magic pill", driving these ruthenium pyrochlores metallic.

IV. CONCLUSIONS

The pyrochlore series $(Pr_{1-x}Bi_x)_2Ru_2O_7$ has been prepared and examined through neutron total scattering techniques to understand the structural role of the *A*-site cation on the compositional insulator-to-metal transition observed across the series. This work explores the simple model that increasing the ionic size of the *A*-site cation will increase the Ru–O–Ru bond angle, which will in turn drive a transition from insulating to metallic behavior. We observe disorder in the form of local Bi off-centering in all Bi-containing compositions, resulting in a larger effective size of the *A*-site, causing a deviation from a linear increase in the Ru–O–Ru bond angle with increasing Bi-content. The increased bond angle produces a wider bandwidth and more effective screening against electron correlation. Electronic structure calculations also point out the first-order effect of the Bi^{3+}: when off-centered, Bi^{3+} decrease the Bi 6p mediated covalency of Ru and O, allowing charge carriers to be further mobilized. Together, these effects drive the insulator-to-metal transition in the Bi-containing members of the solid-solution and explain the non-linear behavior of this dependence. This work highlights the importance of local disorder on transport properties, and suggests that lone pair stereochemical activity could be employed to control insulator-to-metal transitions in pyrochlores and related materials.

ACKNOWLEDGMENTS

G. L. gratefully acknowledges support for this work from Bates College, and from the National Science Foundation (NSF) through DMR 1904980. The work at Northwestern and at UC Santa Barbara was supported by NSF DMR 1729303. The computational contributions of D.P. was supported by the Army Research Office under W911NF-15-1-0017. The use of DOD-HPCMP resources for the computational work reported here is gratefully acknowledged. M. W. G. thanks the Leverhulme Trust for funding via the Leverhulme Research Centre for Functional Materials Design. This work was performed, in part, at the Los Alamos Neutron Science Center (LANSCE), a NNSA User Facility operated for the U.S. Department of Energy (DOE) by Los Alamos National Laboratory (Contract 89233218CNA000001). We thank Joan Siewenie for assistance with NPDF data collection.

* glaurita@bates.edu

[1] M. Foo, W.-L. Lee, T. Siegrist, G. Lawes, A. P. Ramirez, N. Ong, and R. Cava, Mat. Res. Bull. **39**, 1663 (2004).
[2] W. Kobayashi, Phys. Rev. B **79**, 155116 (2009).
[3] T. Toriyama, M. Watanabe, T. Konishi, and Y. Ohta, Phys. Rev. B **83**, 195101 (2011).
[4] A. Pautrat and W. Kobayashi, Europhys. Lett. **97**, 67003 (2012).
[5] T. Taniguchi, T. Munenaka, and H. Sato, J. Phys.: Conf. Ser. **145**, 012017 (2008).
[6] Y. Maeno, H. Hashimoto, K. Yoshida, S. Nishizaki, T. Fujita, J. G. Bednorz, and F. Lichtenberg, Nature **372**, 532 (1994).
[7] Y. Maeno, T. M. Rice, and M. Siegrist, Phys. Today **54**, 42 (2001).
[8] A. Callaghan, C. W. Moeller, and R. Ward, Inorg. Chem. **5**, 1572 (1966).
[9] Y. Noro and S. Miyahara, J. Phys. Soc. Jap. **27**, 518A (1969).
[10] P. T. Barton, R. Seshadri, and M. J. Rosseinsky, Phys. Rev. B **83**, 064417 (2011).

[11] R. G. Egdell, J. B. Goodenough, A. Hamnett, and C. C. Naish, Journal of the Chemical Society, Farad. Trans. **79**, 893 (1983).
[12] H. S. Horowitz, J. M. Longo, H. H. Horowitz, and J. T. Lewandowski, ACS Symp. Ser. **127**, 143 (1985).
[13] T. R. Felthouse, P. B. Fraundorf, M. Friedman, and C. L. Schosser, J. Catal. **127**, 421 (1991).
[14] S. H. Oh, R. Black, E. Pomerantseva, J.-H. Lee, and L. F. Nazar, Nature Chem. **4**, 1004 (2012).
[15] P. F. Garcia, A. Ferretti, and A. Suna, J. Appl. Phys. **53**, 5282 (1982).
[16] M. A. Subramanian, G. Aravamudan, and G. V. Subba Rao, Prog. Solid State Chem. **55**, 55 (1983).
[17] A. W. Sleight, Inorg. Chem. **7**, 1704 (1968).
[18] D. P. Shoemaker, R. Seshadri, M. Tachibana, and A. L. Hector, Phys. Rev. B **84**, 064117 (2011).
[19] D. P. Shoemaker, R. Seshadri, A. L. Hector, A. Llobet, T. Proffen, and C. J. Fennie, Phys. Rev. B **81**, 144113 (2010).
[20] G. Herranz, V. Laukhin, F. Sanchez, P. Levy, C. Ferrater, M. V. Garcia-Cuenca, M. Varela, and J. Fontcuberta, Phys. Rev. B **77**, 165114 (2008).
[21] G. Laurita, R. Grajczyk, M. Stolt, I. Coutinho, A. W. Sleight, and M. A. Subramanian, Inorg. Chem. **55**, 3462 (2016).
[22] R. Seshadri, Solid State Sci. **8**, 259 (2006).
[23] P. W. Anderson, Phys. Rev. **102**, 1008 (1956).
[24] S. T. Bramwell and M. J. P. Gingras, Science **294**, 1495 (2001).
[25] K.-S. Lee, D.-K. Seo, and M.-S. Whangbo, J. Solid State Chem. **131**, 405 (1997).
[26] L. Li and B. Kennedy, Chem. Mater. **15**, 4060 (2003).
[27] F. Ishii and T. Oguchi, J. Phys. Soc. Jap. Japan **69**, 526 (2000).
[28] B. J. Kennedy and T. Vogt, J. Solid State Chem. **126**, 261 (1996).
[29] M. W. Gaultois, P. T. Barton, C. S. Birkel, L. M. Misch, E. E. Rodriguez, G. D. Stucky, and R. Seshadri, J. Phys.: Condens. Matt. **25**, 186004 (2013).
[30] T. Proffen, T. Egami, S. J. L. Billinge, A. K. Cheetham, D. Louca, and J. B. Parise, Appl. Phys. A: Mater. Sci. Process **74**, s163 (2002).
[31] A. C. Larson and R. B. Von Dreele, Los Alamos Nat. Lab. Rep. **LAUR**, 89 (1994).
[32] B. H. Toby, J. Appl. Cryst. **34**, 210 (2001).
[33] P. F. Peterson, M. Gutmann, T. Proffen, and S. J. L. Billinge, J. Appl. Cryst. **34**, 1192 (2000).
[34] C. L. Farrow, P. Juhas, J. W. Liu, D. B. Bryndin, E. S. J. Bloch, T. Proffen, and S. J. L. Billinge, J. Phys.: Condens. Matt. **19**, 335219 (2007).
[35] K. Momma and F. Izumi, J. Appl. Cryst. **44**, 1272 (2011).
[36] J. P. Perdew, A. Ruzsinszky, G. I. Csonka, O. A. Vydrov, G. E. Scuseria, L. A. Constantin, X. Zhou, and K. Burke, phys..
[37] G. Kresse and J. Furthmüller, Comput. Mater. Sci. **6**, 15 (1996).
[38] P. E. Blöchl, O. Jepsen, and O. K. Andersen, phys..
[39] T. Yamamoto, R. Kanno, Y. Takeda, O. Yamamoto, Y. Kawamoto, and M. Takano, J. Solid State Chem. **109**, 24 (2002).
[40] R. J. Bouchard and J. L. Gilson, Mat. Res. Bull. **6**, 669 (1971).
[41] Y. Zhou, I. Matsubara, R. Funahashi, and S. Sodeoka, Mater. Lett. **51**, 347 (2001).
[42] R. Kanno, Y. Takeda, T. Yamamoto, Y. Yamamoto, and O. Yamamoto, J. Solid State Chem. **102**, 106 (1993).
[43] M. Yasukawa, S. Kuniyoshi, and T. Kono, Solid State Comm. **126**, 213 (2003).
[44] R. D. Shannon and C. T. Prewitt, Acta Crystallogr. Sect. B Struct. Crystallogr. Cryst. Chem. **25**, 925 (1969).
[45] S. Muñoz Perez, R. Cobas, J. M. Cadogan, J. Albino Aguiar, P. Bonville, T. Piug, and X. Obradors, J. Appl. Phys. **111**, 07E150 (2012).
[46] R. A. Beyerlein, H. S. Horowitz, and J. M. Longo, J. Solid State Chem. **72**, 2 (1988).
[47] A. W. Sleight and R. J. Bouchard, NBS Special Publication 364: Solid State Chem. , 227 (1972).
[48] M. Avdeev, M. K. Haas, J. Jorgensen, and R. J. Cava, J. Solid State Chem. **169**, 24 (2002).
[49] M. Tachibana, Y. Kohama, T. Shimoyama, A. Harada, T. Taniyama, M. Itoh, H. Kawaji, and T. Atake, Phys. Rev. B **73**, 1098 (2006).
[50] A. L. Hector and S. B. Wiggins, J. Solid State Chem. **177**, 139 (2004).
[51] B. Rehak, K.Horcic, M.Frumar, and L.Koudelka, J. Cryst. Growth **68**, 647 (1984).